

# Chapter 7

## Structure Matters: Combining X-Ray Scattering and Ultraviolet Photoelectron Spectroscopy for Studying Organic Thin Films

Alexander Hinderhofer, Keiichirou Yonezawa, Kengo Kato,  
and Frank Schreiber

### 7.1 Introduction

In this chapter the relationship between organic film structure and ultraviolet photoelectron spectroscopy (UPS) data is discussed. As a useful method for obtaining detailed structural data we first summarize shortly the advantages of X-ray scattering. Here, of course we cannot include the full body of literature on interface-sensitive X-ray scattering but rather refer to general references. By combining such structural data and electronic information from UPS new insights in the fundamental principles of organic electronics can be obtained. On the basis of single layer and heterostructures we discuss the dependence of the electronic level alignment and the spectral shape of the HOMO band on the structural properties of organic thin films. The crystallinity and therefore also the electronic properties of an organic thin film can be tuned by controlling growth parameters such as the substrate temperature. The examples are drawn from our own work in order to specifically relate to other chapters in this book, which is not intended to imply that there are no others [1–3].

---

A. Hinderhofer (✉) • K. Yonezawa • K. Kato  
Department of Nanomaterial Science, Graduate School of Advanced Integration Science,  
Chiba University, Inage-ku, Chiba 263-8522, Japan  
e-mail: [alexander.hinderhofer@chiba-u.jp](mailto:alexander.hinderhofer@chiba-u.jp); [k.yonezawa@chiba-u.jp](mailto:k.yonezawa@chiba-u.jp); [acwa3955@chiba-u.jp](mailto:acwa3955@chiba-u.jp)

F. Schreiber  
Institute for Applied Physics, University of Tübingen, Auf der Morgenstelle 10,  
2076 Tübingen, Germany  
e-mail: [frank.schreiber@uni-tuebingen.de](mailto:frank.schreiber@uni-tuebingen.de)

## 7.2 X-Ray Scattering

### 7.2.1 X-Ray Reflectivity

X-ray reflectivity (XRR) is a powerful tool to probe structure and morphology of organic thin films. Here only the basic concepts of XRR are described. For the details on this method we refer to Refs. [4, 5]. Figure 7.1 depicts the simplified scattering geometry of XRR, for which the angle of incidence  $\Theta$  and the detector angle  $\Omega$  are kept equal:  $\Theta = \Omega$ . Then the complete momentum transfer  $q$  has only a non-zero component perpendicular to the substrate ( $q_z$ ) and can be written as:

$$q_z = \frac{4\pi}{\lambda} \sin \Theta \quad (7.1)$$

Using the Fresnel coefficients the reflectivity  $R$  of a multilayer can be modeled within the framework of dynamical scattering theory with a recursive formalism described by Parratt [6].

The electron density profile of a sample can be extracted along the surface normal by fitting the experimental data. That is, only information about the out-of-plane sample structure is obtained. In Fig. 7.2a a typical XRR dataset from an organic thin film diindenoperylene (DIP) is shown. From fitting such a dataset the following physical parameters, which are actually the free parameters of the fit, can be obtained:

- **Average electron density** The average electron density  $\rho_e$  of a sample is directly connected to the total reflection edge in XRR data.
- **Film thickness** From the periodicity of the Kiessig or thickness oscillations the average thickness  $d$  of a thin film can be determined.
- **Roughness** From the damping of the Kiessig oscillations the roughness  $\sigma_{\text{rms}}$  of a thin film can be determined.
- **Out-of-plane lattice spacing** In organic thin films molecules are often ordered in a crystal, which results in a periodic variation in the electron density of a thin film, from which the out-of-plane lattice spacing can be determined (Fig. 7.2b).

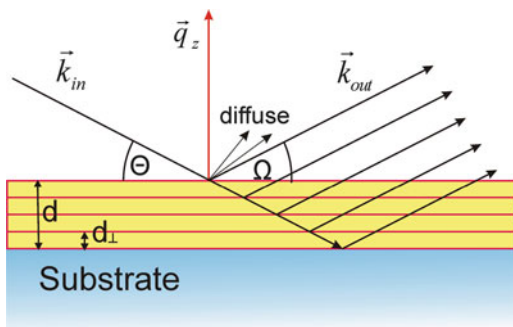


**Fig. 7.1** Scattering geometry for X-ray reflectivity (XRR) on a thin film.  $d$  corresponds to the film thickness and  $d_{\perp}$  is the out-of-plane layer spacing. For XRR the momentum transfer  $q_z$  is perpendicular to the substrate

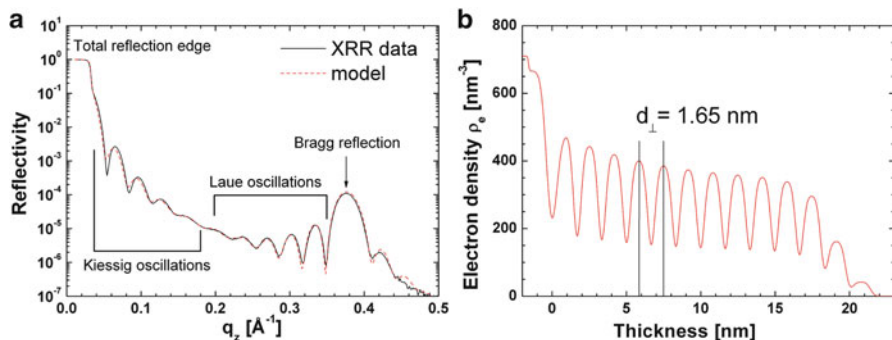


**Fig. 7.2** (a) XRR data from a 20 nm DIP film grown on SiO<sub>2</sub> fitted with a Parratt-model. The fitted electron density versus film thickness is shown in (b)

Since the molecules are often oriented with their long axis along the growth direction the periodicity is on a length scale larger than 1 nm. Constructive interference from waves scattered at the crystal planes gives rise to Bragg reflections at certain angles. The position of Bragg reflections in XRR may be approximated by Bragg's law:

$$n\lambda = 2d_{\perp} \sin \theta \quad (7.2)$$

However, in contrast to scattering from crystal powders, for XRR, the Bragg peak positions may in general be shifted due to multiple scattering.

- **Coherently scattering island size** From the periodicity of the side fringes of the Bragg reflection (Laue oscillations) the coherently scattering crystal size can be determined. If the periodicity of the Laue oscillations and Kiessig oscillations is equal, the film is coherently ordered for the complete film thickness.

Modeling XRR data, such as presented in Fig. 7.2a, with the Parratt-formalism results in a complete electron density profile of a thin film as shown in Fig. 7.2b, from which the thin film parameters described above can be extracted. For organics, the absorption  $\beta$  is in the order of  $1 \times 10^{-9}$ . Thus, for the derivation of the intensity of specularly reflected X-rays from organic thin films  $\beta$  is neglected.

## 7.2.2 Grazing Incidence X-Ray Diffraction

To gain knowledge about lateral structures, grazing incidence x-ray diffraction (GIXD) can be performed. Here, only the main concepts of GIXD are presented, for details it is referred to Ref. [7].

In GIXD, the angle of incidence  $\theta$  is near the total reflection edge with an angle of  $\alpha_c$ . In this case we observe total external reflection and the transmitted wave is

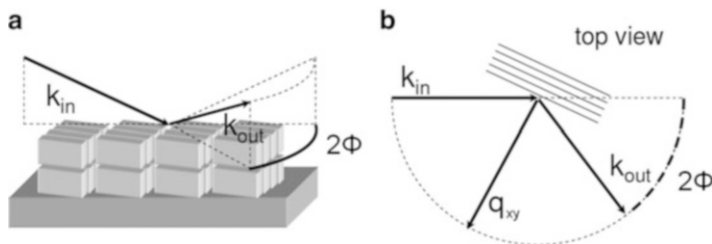


**Fig. 7.3** (a) In GIXD the X-ray beam has an angle of incidence near the critical angle and the detector angle is varied parallel to the substrate by the angle  $2\Phi$ . (b) X-rays are diffracted by the crystalline in-plane lattice by an angle  $2\Phi$ , yielding information about the lattice spacing within the plane. Picture taken and modified from Ref. [8]

very weak. It propagates along the surface with a penetration depth of  $\Lambda = 12k\alpha_c$ , which is the distance at which the intensity falls off by a factor of  $1/e$ . Due to the finite penetration depth, it is called an evanescent wave. For GIXD the out-of-plane detector angle is kept equal to the angle of incidence  $\Omega = \Theta$ . The in-plane crystal structure is probed by varying the in-plane angle  $2\Phi$  related to the in-plane momentum transfer  $q_{xy} \approx 4\pi\lambda \sin \Phi$  (Fig. 7.3).

Samples studied in the following correspond to an in-plane powder. Thus, in the in-plane direction crystalline domains do not have a preferred orientation. However, perpendicular to the sample surface (i.e. out-of-plane), the lattice planes are all oriented parallel to the sample surface. Therefore probing the in-plane structure by GIXD can be understood in terms of powder diffraction. For acquisition of this powder diffraction pattern it is possible to use a point detector and perform a  $2\Phi$  scan. Alternatively, it is possible to use an area detector, thereby acquiring scattering data for a whole range of exit angles in the in-plane direction. With an area detector additional information in the out-of-plane direction  $q_z$  is also resolved. The momentum transfer in each direction is calculated from the following equations:

$$q_{xy} = \frac{2\pi}{\lambda} \sqrt{(\sin \Phi \cos \Omega)^2 + (\cos \Omega \cos \Phi - \cos \Theta)^2} \quad (7.3)$$

$$q_z = \frac{2\pi}{\lambda} (\sin \Theta + \sin \Omega) \quad (7.4)$$

### 7.2.3 Coherent Island Size and Scherrer Formula

The peak width of a Bragg reflection depends on the number lattice planes, which are scattering the incoming X-rays coherently. Lower limits of the coherent in-plane island size  $l_s$  can be determined by the Scherrer formula [5]:

$$l_s = 2\pi/\text{FWHM} \cdot 0.9394 \cdot K_s \quad (7.5)$$

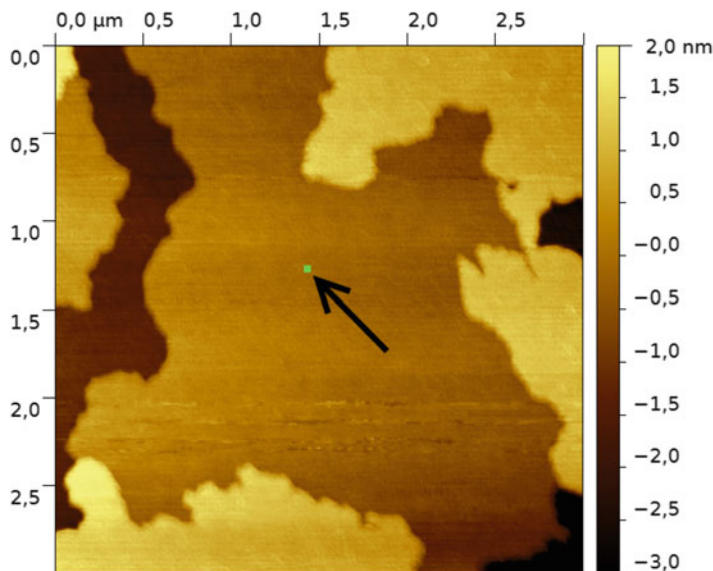


**Fig. 7.4** AFM image of a thin DIP film ( $d \sim 2$  nm) on  $\text{SiO}_2$  showing crystalline islands on the order of several  $\mu\text{m}$ . The *green dot* pointed at by the arrow depicts the average defect free coherent island size  $l_s \sim 30$  nm as determined by GIXD

Here  $K_s = 1.0747$  is the Scherrer constant for spherical grains and FWHM is the full width half maximum of the peak. Here, Eq. 7.5 is mainly used to determine the coherent in-plane island size  $l_s$ . However the same formula could be used to estimate the coherent out-of-plane island size  $l_z$ . When the instrumental broadening of the diffractometer is not included in the calculations, only lower limits of  $l_s$  and  $l_z$  can be obtained.

For organic thin films grown on amorphous substrates like  $\text{SiO}_2$ ,  $l_s$  does often not exceed  $\sim 50$  nm, which is in contrast to the much larger domain sizes visualized by atomic force microscopy (AFM) or X-ray spectromicroscopy [9, 10]. For example Fig. 7.4 shows an AFM image of thin DIP film on  $\text{SiO}_2$  with domain sizes of several  $\mu\text{m}$ . The green dot in this image represents the average defect free coherent island size  $l_s \sim 30$  nm of this sample as determined by GIXD.

### 7.3 Probing Depths of X-Ray Scattering and UPS

When combining data from different methods always care have to be taken. Both X-ray scattering and UPS have usually a rather large probing area in the range of  $\text{mm}^2$ . However, the probing depths of both methods depend on different parameters and can be very different.

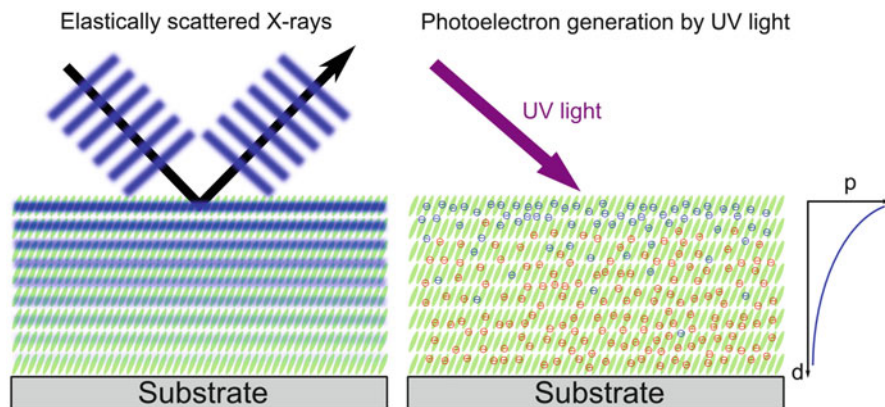


**Fig. 7.5** Illustration of probing depth for GIXD (*left*) and UPS (*right*). For GIXD, the intensity of the evanescent wave decays exponentially from the surface dependent on photon energy and angle of incidence. For UPS the probability  $p$  of generated photoelectrons to leave the sample unscattered decreases exponentially for larger film thicknesses  $d$ . For example the “blue” electrons may leave the film unscattered, while the “red” electrons will be scattered inelastically before reaching the film surface

For UPS the probing depth is limited by inelastic mean free path IMFP of the generated photoelectrons, i.e. the average length a free electron can travel in the film before it is scattered inelastically. The IMFP depends mainly on the kinetic energy of the electron transferred from an incident photon and does only weakly depend on the material. The IMFP for different kinetic energies is therefore often presented as a “universal curve” valid for all materials. Since the penetration depth of the incident UV-light is usually much larger than the IMFP of the excited photoelectrons we assume that the amount of electrons generated is nearly equal at all thicknesses through the film. Then, as illustrated in Fig. 7.5, the probability  $p$  for an electron to reach the surface without being inelastically scattered decreases exponentially with larger distances  $d$  between surface and place of generation.

In contrast to UPS, the probing depth of X-ray scattering techniques depend on photon energy, angle of incidence and the dielectric function of the thin film. For most scattering geometries, for example XRR, the angle of incidence relative to the sample surface is above the total reflection edge. Thus the X-ray beam is penetrating completely into the sample until it is absorbed or reflected, resulting in a probing depth which is usually much larger than the film thickness. For GIXD, the angle of incidence is below the total reflection edge, which means that the X-ray beam is totally reflected at the surface and only an evanescent wave, with exponentially decreasing intensity (Fig. 7.5) is penetrating into the film. By adjusting the angle of incidence (or photon energy) for a given sample the probing depth can be varied, but due to the intensity decay versus thickness the signal-weight is always biased to the surface area, similar as is the case for UPS.

## 7.4 Example 1: DIP at Different Substrate Temperatures

The structure of organic semiconductor thin films is frequently modified by varying the substrate temperature during deposition to tune the electrical and optical characteristics of the films. In general, at high substrate temperatures ( $T$ ) molecular mobilities are high leading to enhanced crystallinity and grain size in the grown films [2, 11]. In contrast, deposition at low temperatures is applied to obtain less crystalline or amorphous films [9, 12–17]. For low  $T$  growth, it is often not clear, if the film undergoes a structural or morphological transition upon heating to room temperature, because characterization is mostly done after growth at room temperature. In particular, properties like crystallinity, molecular orientation and roughness of the film surface are important for device applications with organic heterostructures, where the top surface of the first layer serves as a template for subsequent layers [3, 18, 19].

Here, we study the morphological and electronic impact of post-growth heating on low  $T$  deposited organic thin films by X-ray reflectivity (XRR) and ultraviolet photoelectron spectroscopy (UPS). For the experiments we choose diindeno-perylene (DIP,  $C_{32}H_{16}$ , inset Fig. 7.6b) as an organic material with high relevance for applications [20–23]. For example, organic solar cells with DIP as electron donor reached high fill factors and power conversion efficiencies of more than 4%. DIP is deposited on two different substrates (indium-tin-oxide (ITO) and silicon dioxide ( $SiO_2$ )), because the film characteristics on both substrates differ in crystallinity [15, 16]. X-ray diffraction techniques [5] were applied to determine the bulk crystal structure and surface roughness ( $\sigma_{RMS}$ ). UPS was used to determine the surface electronic structure, which depends on the crystallinity, orientation and

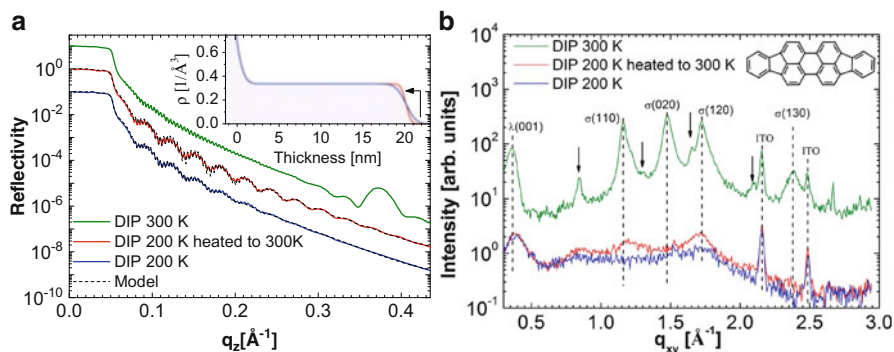


**Fig. 7.6** (a) XRR and (b) GIXD data of a DIP film ( $d = 20$  nm) grown on ITO at 200 K measured directly after growth at 200 K and after slow heating ( $\sim 1$  h) to 300 K. For comparison, data from a film grown and measured at 300 K is also shown. The inset in (a) shows the modeled electron density of the 200 K film directly after growth (blue) and after heating (red). The inset in (b) shows the molecular structure of DIP. Reprinted with permission from Ref. [31]

uniformity of domains at the surface [24–26]. The combination of both techniques, therefore, provides information on the change of structure and morphology of the films for the entire thickness region.

### 7.4.1 Experimental

Organic thin films of DIP were grown on silicon wafers with native SiO<sub>2</sub> (surface roughness  $\sigma_{\text{RMS}} = 0.3$  nm) or on ITO-coated glass substrates (ITO thickness: 130 nm,  $\sigma_{\text{RMS}} = 0.95$  nm) under ultra high vacuum (UHV) conditions (base pressure  $< 6 \cdot 10^{-9}$  mbar) by thermal evaporation. Before deposition, substrates were cleaned ultrasonically with acetone, isopropanol, and ultra pure water, followed by heating to 700 K in the UHV growth chamber. The growth rate was between 0.1 and 0.3 nm/min monitored by XRR and a quartz crystal microbalance. Substrate temperatures during growth and measurements were controlled with liquid nitrogen cooling in a range of  $T = 200 - 300$  K.

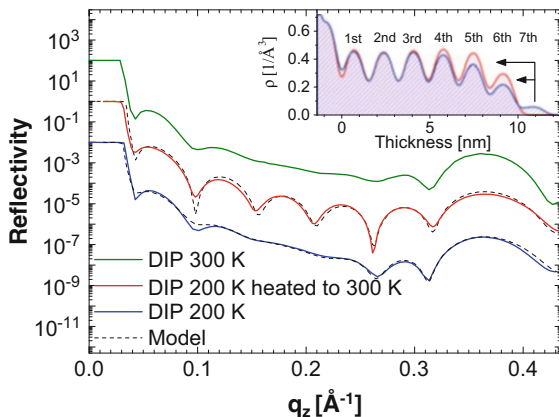
In situ XRR and grazing incidence X-ray diffraction (GIXD) for the ITO samples were performed at beamline ID10B ( $\lambda = 0.092$  nm) of the ESRF in Grenoble, France. XRR for SiO<sub>2</sub> samples were performed at the X04SA beamline of the Swiss Light Source, Paul Scherrer Institut, Villigen, Switzerland ( $\lambda = 0.10$  nm). Peak indexing of DIP is based on the crystal structure (P21/a polymorph) reported in Ref. [27]. Modeling of XRR data was done with Motofit [28].

He I UPS experiments were performed with a home-built UHV system equipped with a PHOIBOS-HSA100 analyzer with an energy resolution of 60 meV [29]. UPS were measured at a light incident angle of 45° and electron emission angles of 0° (normal emission). After growth in a UHV preparation chamber the samples were directly transferred to the measurement chamber without breaking the vacuum and with keeping the substrate temperature at 200 K. The vacuum level (VL) was obtained by applying a sample bias of  $-5$  V during the UPS measurements.

### 7.4.2 Results

Figure 7.6a shows XRR data from a DIP film with a thickness of  $d = 20$  nm grown on ITO at 200 K and measured at 200 K directly after growth and after slow heating ( $\sim 1$  h) to 300 K. Both films show no out-of-plane Bragg reflections, indicating weak order in this direction. We applied a three layer model (glass-ITO-DIP) to fit the electron densities  $\rho$  of the as-grown and the annealed films (inset Fig. 7.6a). From the electron densities of both films it is evident that the roughness is reduced by 50 % during annealing from initially  $\sigma_{\text{RMS}} = 0.90$  nm to  $\sigma_{\text{RMS}} = 0.45$  nm at 300 K. For comparison, XRR from a film grown and measured at 300 K is also shown. This film is crystalline and exhibits an out-of-plane lattice spacing of 1.69 nm corresponding to textured growth of the strained high temperature

**Fig. 7.7** XRR data of DIP films ( $d = 10$  nm) grown on  $\text{SiO}_2$  at two different substrate temperatures (200 K and 300 K). For the 200 K DIP film, XRR data directly after growth at 200 K are shown together with data after slow heating ( $\sim 1$  h) to 300 K. The inset shows the modeled electron density of the 200 K film directly after growth (*blue*) and the heated 200 K film (*red*). Reprinted with permission from Ref. [31]



phase of DIP (HT-phase) [27, 30] with the (001) plane parallel to the substrate ( $\sigma$ -structure). The roughness of this film is significantly higher compared to low  $T$  deposited films ( $\sigma_{RMS} = 2.6$  nm).

Figure 7.6b shows GIXD data of the 200 K DIP film on ITO before and after heating. Before heating the film shows only very broad Bragg reflections with the most intense feature stemming from domains with nearly lying DIP molecules ( $\lambda(001)$  of the HT-phase). During heating the film crystallizes partly in the DIP HT-phase as seen by the slight intensity increase of the  $\sigma(110)$  and  $\sigma(120)$  reflections. However, all reflections both from the  $\lambda$ - and  $\sigma$ -structure remain broad with a coherent island size of less than 5 nm estimated with the Scherrer formula [5]. GIXD data from a crystalline film grown and measured at 300 K (Fig. 7.6b) exhibits mainly Bragg reflections corresponding to textured growth of the DIP HT-phase ( $\sigma$ -structure) [27]. Bragg reflections marked with stars stem presumably from a DIP low temperature phase as suggested in Refs. [15, 16, 27]. XRR and GIXD data show that during heating to room temperature the bulk DIP film on ITO crystallizes only partly, however, the reorganization of the surface molecules yield a very low roughness.

In Ref. [15] it was shown that low  $T$  deposition of DIP on  $\text{SiO}_2$  yield films, which are more crystalline than films deposited on rough substrates like ITO. In the following, we report on an in situ study of such a film, in order to test if the surface smoothing observed for amorphous DIP films on ITO is also present for crystalline films upon heating to room temperature.

Figure 7.7 shows XRR data from a DIP film ( $d = 10$  nm) grown on  $\text{SiO}_2$  at 200 K measured at 200 K directly after growth and after slow heating to 300 K. From the modeled electron densities of the heated and the as-grown 200 K DIP film (inset Fig. 7.7) we find that both films are crystalline and exhibit an out-of-plane lattice spacing of 1.69 nm corresponding again to textured growth of the strained DIP HT-phase ( $\sigma$ -structure) [27, 30]. However, the layer fillings of these films show

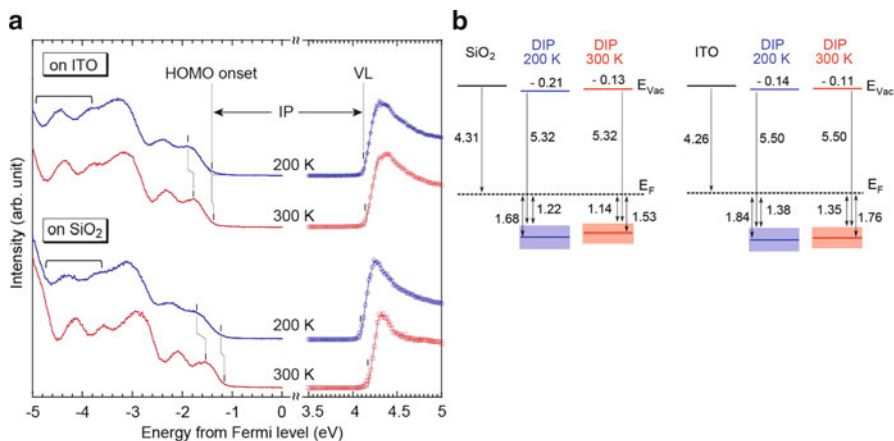


**Fig. 7.8** (a) UPS data of DIP films grown on SiO<sub>2</sub> ( $d = 10$  nm) and ITO ( $d = 20$  nm) at 200 K and after slow heating ( $\sim 4$  h) to 300 K. (b) Schematic energy level diagram. The HOMO width is given by the difference of the HOMO peak position and the HOMO onset. Reprinted with permission from Ref. [31]

significant differences (inset Fig. 7.11), resulting in roughnesses of  $\sigma_{RMS} = 1.5$  nm for the as-grown film and  $\sigma_{RMS} = 0.75$  nm for the heated film. This observation is rationalized by a molecular ‘downhill’ current from the top layer (7th) to the partly filled lower lying layers (6th, 5th, 4th), thereby leaving the out-of-plane crystal structure and the intermediate electron density unchanged. For comparison, XRR from a film grown and measured at 300 K is also shown. This film has the same out-of-plane lattice spacing (1.69 nm) and a similar roughness as the 200 K film without annealing ( $\sigma_{RMS} = 1.6$  nm).

The observation of the roughness reduction by  $\sim 50\%$  shows that the reorganization of surface molecules is not exclusively a feature of amorphous films. Surprisingly, also for a bulk crystalline film deposited at low  $T$  the surface is smoothed upon heating.

### 7.4.3 UPS

We employed UPS to detect the correlation between structure and the molecular electronic states upon heating, since the electronic states near the surface play a significant role in the energy level alignment of organic heterostructures. The probing depth of UPS is  $\sim 1$  nm, which means that the bulk of the film does not contribute to the measured data. Figure 7.8 shows UPS data of DIP films prepared under similar conditions as those as presented above. The ionization potential (IP) of DIP (200 K) on SiO<sub>2</sub> (5.32 eV) and on ITO (5.5 eV) was

determined from the onset of the highest occupied molecular orbital (HOMO) and the vacuum level (VL). The IP of DIP depends on the orientation of the molecules at the surface [32]. An IP of 5.32 eV is consistent with a nearly upright oriented DIP film [20, 33]. The IP of lying DIP is larger by  $\sim 0.4$  eV compared to nearly upright standing DIP as was shown in Refs. [34–36]. The DIP film on ITO is nearly amorphous and exhibits therefore no preferred molecular orientation. In addition, the size of orientational domains is very small, which results in a common vacuum level. Consistently, the IP of 5.5 eV of this film corresponds to an average of standing and lying DIP.

After heating the IP of both films did not change significantly, indicating that the DIP molecules did not reorient on average. However we detect a parallel shift of all valence features towards the Fermi level, which is attributed partly to an interfacial dipole effect and partly to the reduction of gap states (Fig. 7.8b). Dipole effects are associated with a parallel shift of the HOMO and the vacuum level. A HOMO shift stemming from a reduction of gap states is recognized by a reduced peak width of the valence states (gap state effect). For DIP on SiO<sub>2</sub> (ITO) the HOMO shift is  $\Delta E = 0.15$  eV ( $\Delta E = 0.08$  eV) with a contribution of 0.08 eV (0.03 eV) from the dipole effect and 0.07 eV (0.05 eV) from the gap state effect. The dipole effect may be attributed either to an interfacial dipole between the surface layer and its underlayer induced by a slightly different electron density at the interface [37], and/or a temperature dependent level alignment between the substrates and the DIP. The spectral broadening at low  $T$  is caused by different polarization environments associated with disorder of the molecules at the nearest-neighbor level. The peak narrowing upon heating indicates therefore that the surface molecules are more uniformly ordered for both systems which results in more similar polarization environments for them. Since the density of gap states is reduced, the HOMO level shifts closer to the Fermi level. This effect is explained in detail in Refs. [38–40].

When comparing the DIP-on-SiO<sub>2</sub> and the DIP-on-ITO systems several differences can be found as shown in Fig. 7.9: First, at 200 K molecules at the film surface on SiO<sub>2</sub> orient basically nearly upright ( $\sigma$ -orientation), which is consistent with the data in Fig. 7.6. Nevertheless, at this temperature the spectral features of DIP-on-SiO<sub>2</sub> exhibit a similar or even stronger broadening compared to DIP-on-ITO, which can be observed most easily from the energy region around  $-4$  eV marked with brackets in Fig. 7.8. The broad spectrum of DIP-on-SiO<sub>2</sub> implies that, in spite of better bulk crystallinity, the surface material in films on SiO<sub>2</sub> does not show a better in-plane order than DIP-on-ITO. Second, upon heating peak narrowing and the spectral shift are both significantly more pronounced for the DIP-on-SiO<sub>2</sub> system compared to the DIP-on-ITO system. This implies that the ordering effect of the surface material is more pronounced if the crystallinity of the initial material is better, which is the case for DIP-on-SiO<sub>2</sub> (Fig. 7.9).

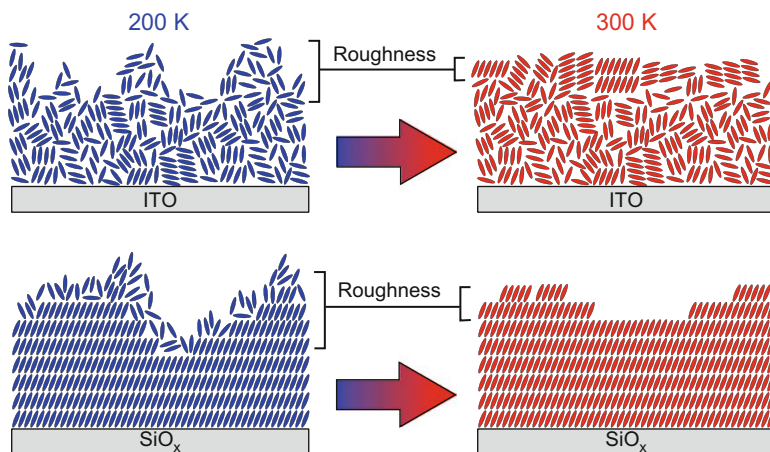


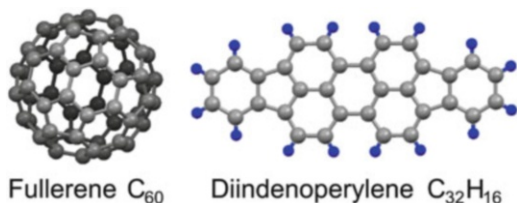
**Fig. 7.9** A sketch of DIP thin films on ITO and  $\text{SiO}_2$  illustrating the surface smoothing due to crystallization upon heating. Reprinted with permission from Ref. [31]

## 7.5 Example 2: $\text{C}_{60}$ on DIP

For growth of organic thin films the structure and morphology depends strongly on the substrate, onto which they are deposited [2, 41]. This was demonstrated for example by the surface modification of an inorganic substrate with an organic self assembled monolayer (SAM), which influenced the resulting growth behavior [42–49]. For such heterostructures the growth behavior of the top layer is mostly discussed in terms of surface energies, although also some degree of azimuthal alignment has been observed [49]. In contrast, a close relationship between two organic layers can be observed in organic-organic heteroepitaxy [3, 18, 50–52]. There, the growth behavior of the deposited compound depends on the, usually anisotropic, potential surface of both involved materials. The control of the top layer morphology by tuning of the bottom layer was also discussed as templating, particularly for changing the molecular orientation relative to the surface (standing orientation vs. lying orientation) [16, 53].

The structural relationship at an organic-organic hetero-interface resulting from the non-equilibrium growth process has a large impact on electrical properties, *inter alia* charge carrier generation and transport [1, 54]. For example for organic field effect transistors it was shown that an organic templating layer may improve the electronic mobility of the active material substantially [18, 55–57]. In this regard, an important point for small-molecule organic semiconductors can be the orientation of the molecules. Frequently, there is at least a competition between lying down and standing up orientation [35, 45], which depends strongly on the underlying substrate. Other systems, such as PTCDA exhibit a very strong tendency to form lying-down structures, almost independent of the substrate [17, 49, 58–60]. In this context,  $\text{C}_{60}$  is a rather unique case in the area of small-molecule organic

**Fig. 7.10** Sketch of fullerene  $C_{60}$  and diindenoperylene (DIP,  $C_{32}H_{16}$ ). Reprinted with permission from Ref. [71]



semiconductors, since it exhibits essentially rotational symmetry. The issue of lying-down vs. standing-up orientation does not complicate matters, and the orientational degrees of freedom in structure formation enter basically only via the orientation of the lattice planes and their distribution or alignment.  $C_{60}$  was shown to grow with low structural order on several inorganic substrates like  $SiO_2$  [61], quartz glass [62] and sapphire [55] but crystallizes well on organics like pentacene [55, 63] or sexiphenyl [64, 65].

Here, we study the influence of a diindenoperylene (DIP, Fig. 7.10) templating layer [27, 30, 66–68] on the growth and electronic structure of  $C_{60}$ . The combination of  $C_{60}$  and DIP in a heterostructure was shown to exhibit excellent photovoltaic performance [20, 69], which is related to the high exciton diffusion length in DIP [23, 70] and the favorable energy level alignment of both materials [20, 21, 33]. In addition, we investigate to which extent structural properties like roughness, domain size and crystallinity of the DIP templating layer influence the growth of  $C_{60}$ .

To study the structure of  $C_{60}$  thin films we compare first a reciprocal space map of a  $C_{60}$  film grown on  $SiO_2$  ( $C_{60}/SiO_2$ ; Fig. 7.11a) with data from  $C_{60}$  grown on DIP ( $C_{60}/DIP$ ; Fig. 7.11b). The  $C_{60}/SiO_2$  film exhibits broad diffraction rings indicating crystalline domains without preferred orientation. Indexing is done according to the  $C_{60}$  *fcc*-structure reported in Ref. [72]. One reflection, indexed as  $C_{60}\#$  in the bottom GIXD data, does not stem from the  $C_{60}$  *fcc*-structure. Its  $q$ -value ( $q = 0.725 \text{ \AA}^{-1}$ ) coincides with the (100) reflection from the  $C_{60}$  *hcp* structure. This observation is in agreement with single crystal growth, where a small fraction of crystals adopt *hcp* packing [72]. Note that in the indexing of GIXD data at the bottom of Fig. 7.11a only one index for each reflection is given, since other reflections with the same  $|q|$  cannot be distinguished. The scattering data of the  $C_{60}/SiO_2$  film shown here is in agreement with data presented in Ref. [61].

Figure 7.11b displays 2-dimensional GIXD data from a  $C_{60}/DIP$  heterostructure. At the bottom the integrated GIXD intensity is shown. Indexing is done again according to the  $C_{60}$  *fcc*-structure. Compared to  $C_{60}$  grown on  $SiO_2$  (Fig. 7.11a) the diffraction pattern of  $C_{60}$  grown on DIP shows significant differences. The distribution of Bragg reflections reveals the alignment of the *fcc*-(111) crystal plane parallel to the substrate. Only a small fraction of crystallites nucleates with a random orientation as indicated by the weak  $C_{60}$  (111)\* index. Note that the Bragg reflection at  $q_{xy} = 0.725 \text{ \AA}^{-1}$  stems not from the *hcp*-structure as in Fig. 7.11a. Instead, this peak is the projection of the *fcc*-(11-1) Bragg reflection onto the  $q_{xy}$  plane. The width of the *fcc* Bragg reflections in  $q_z$  (out-of-plane) is

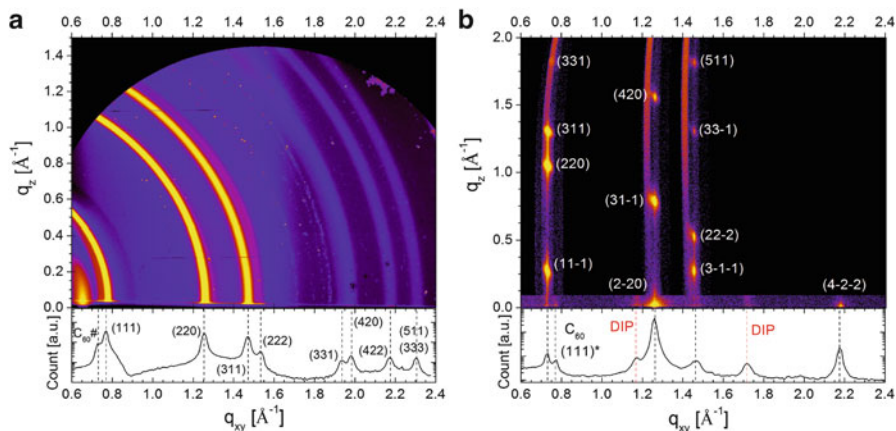


**Fig. 7.11** (a) Reciprocal space map from a 60 nm  $C_{60}$  film recorded with a MARCCD area detector. At the bottom additional GIXD data measured with a point detector at  $q_z = 0.02 \text{ \AA}^{-1}$  is shown. (b) 2-dimensional GIXD data from a 15 nm  $C_{60}$  film grown on a DIP templating layer ( $d = 4 \text{ nm}$ ) indexed according to the  $C_{60}$  *fcc*-structure. The data consist of four detector scans at a fixed angle of incidence at  $0.1^\circ$  performed with a PILATUS II area detector. Images from each data point were transformed into  $q$  coordinates and then assembled into one image. One scan was performed parallel to the substrate plane, for which at the bottom the integrated GIXD data is shown. Three scans were performed along the  $C_{60}$  crystal truncation rods. Reprinted with permission from Ref. [71]

relatively large because of the small crystal size in  $q_z$  direction limited by the film thickness of 15 nm. The in-plane coherent crystal sizes  $l_s$  of both  $C_{60}$  films were determined with the Scherrer formula to be  $l_s = 7 \text{ nm}$  for the  $C_{60}/\text{SiO}_2$  film and  $l_s = 28 \text{ nm}$  for the  $C_{60}/\text{DIP}$  film. For the determination of  $l_s$  of both  $C_{60}$  films we choose the (2-20) and (4-2-2) reflections and averaged over the obtained values. The difference in  $l_s$  is a clear evidence for the improved crystal quality and reduction of crystal defect density in the  $C_{60}/\text{DIP}$  film compared to the  $C_{60}/\text{SiO}_2$  film.

### 7.5.1 UPS

Since  $C_{60}/\text{DIP}$  films are highly relevant for photovoltaic applications [20], we study whether the templating effect demonstrated above influences the electronic structure of  $C_{60}$ .

Figure 7.12a shows UPS data of the highest occupied molecular orbital (HOMO) region of  $C_{60}$  grown on DIP and  $\text{SiO}_2$ . The overall shape of the HOMO and HOMO-1 states in Fig. 7.12a correspond to spectra measured for  $C_{60}$  thin films on various inorganic and organic substrates/films [63, 75–77]. The similarity to the gas phase spectra of  $C_{60}$  [78] indicates only weak interaction between molecules in the thin film. Apart from a spectral shift of 150 meV, resulting from the different energy level

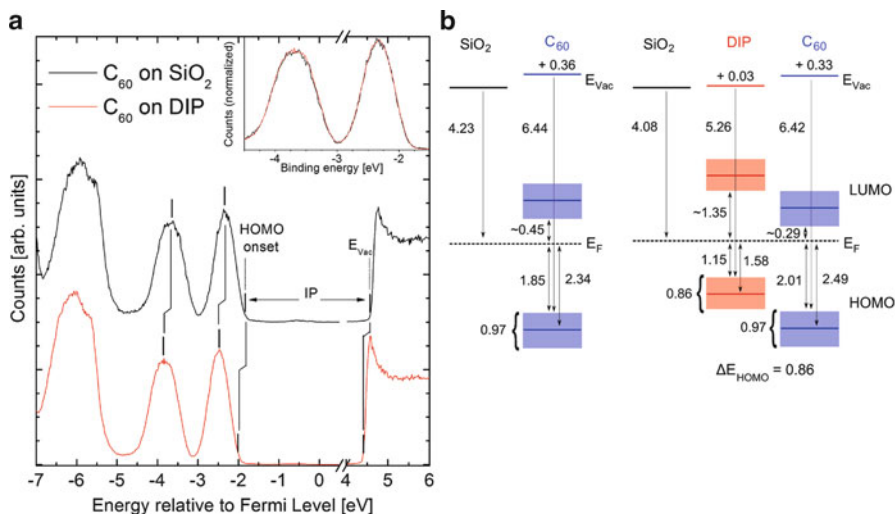


**Fig. 7.12** (a) UPS data from  $C_{60}$  ( $d = 13$  nm) grown on  $SiO_2$  and grown on DIP ( $d = 4$  nm). The inset shows the normalized HOMO regions of both datasets with the  $C_{60}$ /DIP data shifted by 150 meV. (b) Sketch of the electronic level alignment from the UPS data in (a). LUMO levels were taken from Refs. [73, 74]. All values are given in eV and have an error bar of  $\pm 0.05$  eV. The width of the HOMO state is determined by the respective onsets. Reprinted with permission from Ref. [71]

alignment (ELA) of the  $C_{60}$  film to the DIP layer and the  $SiO_2$  substrate, both spectra from the  $C_{60}$  films are essentially identical. This can be seen more clearly in the inset in Fig. 7.12a, where the data are overlaid and the  $C_{60}$ /DIP data were shifted by 150 meV. In addition, also the ionization potentials (IP) determined by the secondary electron cutoff and the HOMO onset are equal (6.4 eV) for both  $C_{60}$  films. Strong changes in structure and domain orientation for organic thin films lead to a significant change in spectral width of the HOMO or the IP depending on the molecular system [31, 32, 79]. However, our data demonstrates that at room temperature thin films of  $C_{60}$  do not show these effects because of the reasons described below.

In general several mechanisms may influence the HOMO-band width of a molecular material [24, 80]. For instance in a non-uniform or disordered film the polarization energy (final state effect) and the intermolecular interaction (initial state effect) is locally different, resulting in slightly different ionization energies at different positions and therefore in spectral broadening. Another broadening effect is associated with band dispersion due to delocalization of the electronic states, which can be observed only for large single crystals of  $C_{60}$  [81] and can therefore be omitted in the following discussion. In comparison to the  $C_{60}/SiO_2$  film we may expect spectral sharpening for the  $C_{60}$ /DIP film, because of the improved crystal quality. The island size of the  $C_{60}/SiO_2$  film is much smaller compared to the  $C_{60}$ /DIP film, implying that the density of crystal defects is higher in the  $C_{60}/SiO_2$  film compared to the  $C_{60}$ -on-DIP film. However, the absence of any difference in

the width of the  $C_{60}$  states implies that a small coherent island size in a  $C_{60}$  film has no significant impact on the polarization energy/intermolecular interaction. This observation may be rationalized by the high-symmetry shape of the single  $C_{60}$  molecule and its rotation at room temperature [76, 82], which results in a much smaller local polarization/interaction variation due to crystal defects in comparison to anisotropic rod-like molecules.

For the mechanisms of energy level alignment at the organic-inorganic and organic-organic interfaces several different models have been discussed [39, 83–88] without a definitive conclusion in the literature. Figure 7.12b summarizes the ELA of two measured samples. For a low work function substrate like  $SiO_2$  ( $WF = 4.23$  eV) the  $C_{60}$  LUMO (lowest unoccupied molecular orbital) level is presumably located at the substrate Fermi level leading to an interface dipole of 0.36 eV. For organic-organic heterostructures the ELA of the top layer is typically governed by the energetic position of the bottom layer. The difference of the HOMO onsets of DIP and  $C_{60}$  as determined here is  $\Delta E_{HOMO} = 0.86$  eV, similar to values reported for a DIP/ $C_{60}$  heterostructure on PEDOT:PSS [20] and for the vice versa heterostructure (DIP-on- $C_{60}$ ) [33].

## 7.6 Summary

In summary, we presented two studies on how X-ray scattering can be combined with UPS to obtain detailed insights in the properties of organic thin films:

In the first example we observed the surface smoothing of low  $T$  deposited organic thin films upon heating to room temperature. With the combined results from X-ray scattering and UPS we illustrated the process of surface smoothing by crystallization as in Fig. 7.9. After low  $T$  deposition on ITO, the DIP film is nearly amorphous and also rough. Upon heating the surface material is crystallizing in domains without any predominant texture, whereas the bulk material does not strongly reorganize, because of lower mobility of these molecules. This crystallization process is associated with a molecular “downhill” current, which smooths the surface. In contrast to deposition on ITO, the DIP film deposited on  $SiO_2$  is, except for the top surface material, already crystalline with a preferred orientation of the domains ( $\sigma$ -orientation). Upon heating to room temperature, the surface material is also crystallizing and exhibits thereby a similar smoothing as the film on ITO. Therefore, we conclude that the smoothing effect observed is qualitatively irrespective of the degree of bulk crystallinity. In addition, due to the crystallization the density of gap states at the surface is changed leading to a shift of the valence band features towards the Fermi level. The observed post-growth smoothing and crystallization is of importance for the growth of organic heterostructures, where the top surface of the first layer serves as a template for subsequent layers.

In the second example we demonstrated that the structural order of  $C_{60}$  is significantly improved by inserting a DIP templating layer between the  $SiO_2$  substrate and  $C_{60}$  film. In contrast to growth on an amorphous substrate like  $SiO_2$ ,

C<sub>60</sub> grown on a DIP film exhibits alignment of *fcc*-domains with the (111) plane parallel to the substrate and a significant increase of the coherent in-plane island size  $l_s$  by a factor of  $\sim 4$ . UPS measurements revealed that the spectral broadening of the C<sub>60</sub> HOMO region interestingly do not depend significantly on the structural order in the C<sub>60</sub> film. This observation is in strong contrast to the data presented in the first example study where an increased of structural order in DIP lead to a significant sharpening of the HOMO band. This unusual behavior can be rationalized by the highly symmetric shape of the C<sub>60</sub> molecule.

**Acknowledgements** The authors thank T. Hosokai, F. Bussolotti and S. Duham for helpful discussions and P. Willmott and S. Leake at the Swiss Light Source whose great efforts have made these experiments possible. This research project has been supported by the DFG, the G-COE program at Chiba University. A.H. acknowledges support from the JSPS.

## References

1. W. Brütting, S. Berleb, A.G. Mückl, *Organic Electronics* **2**(1), 1 (2001). URL <http://www.sciencedirect.com/science/article/B6W6J-42SXF0X-1/1/e711a4bc688f027357e9b1b2be2ab1d7>
2. G. Witte, C. Wöll, *J. Mater. Res.* **19**(7), 1889 (2004). DOI [10.1557/JMR.2004.0251](https://doi.org/10.1557/JMR.2004.0251)
3. A. Hinderhofer, F. Schreiber, *ChemPhysChem* **13**(3), 628 (2012). DOI [10.1002/cphc.201100737](https://doi.org/10.1002/cphc.201100737). URL <http://dx.doi.org/10.1002/cphc.201100737>
4. J. Als-Nielsen, D. McMorrow, *Elements of Modern X-ray Physics* (Wiley, New York, 2001)
5. M. Birkholz, *Thin Film Analysis by X-Ray Scattering* (Wiley-VCH, Weinheim, 2006)
6. L.G. Parratt, *Phys. Rev.* **95**, 359 (1954)
7. H. Dosch, *Critical Phenomena at Surfaces and Interfaces: Evanescent X-Ray and Neutron Scattering* (Springer, Berlin, 1992)
8. S. Kowarik, Real-time studies of thin film growth of organic semiconductors. Ph.D. thesis, Wadham College, Oxford (2006)
9. R. Matsubara, M. Sakai, K. Kudo, N. Yoshimoto, I. Hirokawa, M. Nakamura, *Organic Electronics* **12**, 195 (2011)
10. S. Kowarik, K. Broch, A. Hinderhofer, A. Schwartzberg, J.O. Osso, D. Kilcoyne, F. Schreiber, S.R. Leone, *J. Phys. Chem. C* **114**(30), 13061 (2010). DOI [10.1021/jp103713z](https://doi.org/10.1021/jp103713z). URL <http://pubs.acs.org/doi/abs/10.1021/jp103713z>
11. W. Brütting (ed.), *Physics of Organic Semiconductors* (Wiley-VCH, Weinheim, 2005)
12. D. Käfer, C. Wöll, G. Witte, *Appl. Phys. A* **95**(1), 273 (2009). URL <http://dx.doi.org/10.1007/s00339-008-5011-3>
13. C.D. Dimitrakopoulos, P.R.L. Malenfant, *Adv. Mater.* **14**, 99 (2002)
14. K. Walzer, B. Maennig, M. Pfeiffer, K. Leo, *Chem. Rev.* **107**(4), 1233 (2007). DOI [10.1021/cr050156n](https://doi.org/10.1021/cr050156n). URL <http://pubs.acs.org/doi/abs/10.1021/cr050156n>
15. S. Kowarik, A. Gerlach, S. Sellner, L. Cavalcanti, O. Kononov, F. Schreiber, *Appl. Phys. A* **95**(1), 233 (2009). URL <http://dx.doi.org/10.1007/s00339-008-5012-2>
16. A. Hinderhofer, T. Hosokai, C. Frank, J. Novák, A. Gerlach, F. Schreiber, *J. Phys. Chem. C* **115**, 16155 (2011)
17. B. Krause, F. Schreiber, H. Dosch, A. Pimpinelli, O.H. Seeck, *Europhys. Lett.* **65**(3), 372 (2004). URL <http://stacks.iop.org/0295-5075/65/i=3/a=372>
18. J. Yang, D. Yan, *Chem. Soc. Rev.* **38**, 2634 (2009). DOI [10.1039/B815723P](https://doi.org/10.1039/B815723P). URL <http://dx.doi.org/10.1039/B815723P>

19. A. Hinderhofer, A. Gerlach, S. Kowarik, F. Zontone, J. Krug, F. Schreiber, *EPL* **91**(5), 56002 (2010). DOI [10.1209/0295-5075/91/56002](https://doi.org/10.1209/0295-5075/91/56002). URL <http://stacks.iop.org/0295-5075/91/i=5/a=56002>
20. J. Wagner, M. Gruber, A. Hinderhofer, A. Wilke, B. Bröker, J. Frisch, P. Amsalem, A. Vollmer, A. Opitz, N. Koch, F. Schreiber, W. Brütting, *Adv. Funct. Mater.* **20**, 4295 (2010). URL <http://dx.doi.org/10.1002/adfm.201001028>
21. U. Hörmann, J. Wagner, M. Gruber, A. Opitz, W. Brütting, *Phys. Stat. Sol. (RRL)* **5**(7), 241 (2011). DOI [10.1002/pssr.201105238](https://doi.org/10.1002/pssr.201105238). URL <http://dx.doi.org/10.1002/pssr.201105238>
22. M. Horlet, M. Kraus, W. Brütting, A. Opitz, *Appl. Phys. Lett.* **98**(23), 233304 (2011). DOI [10.1063/1.3598423](https://doi.org/10.1063/1.3598423). URL <http://link.aip.org/link/?APL/98/233304/1>
23. D. Kurrle, J. Pflaum, *Appl. Phys. Lett.* **92**(13), 133306 (2008). DOI [10.1063/1.2896654](https://doi.org/10.1063/1.2896654). URL <http://link.aip.org/link/?APL/92/133306/1>
24. N. Ueno, S. Kera, *Prog. Surf. Sci.* **83**(1012), 490 (2008). DOI [10.1016/j.progsurf.2008.10.002](https://doi.org/10.1016/j.progsurf.2008.10.002). URL <http://www.sciencedirect.com/science/article/pii/S0079681608000567>
25. H. Ishii, K. Sugiyama, E. Ito, K. Seki, *Adv. Mater.* **11**(8), 605 (1999). DOI [10.1002/\(SICI\)1521-4095\(199906\)11:8<605::AID-ADMA605>3.0.CO;2-Q](https://doi.org/10.1002/(SICI)1521-4095(199906)11:8<605::AID-ADMA605>3.0.CO;2-Q). URL [http://dx.doi.org/10.1002/\(SICI\)1521-4095\(199906\)11:8<605::AID-ADMA605>3.0.CO;2-Q](http://dx.doi.org/10.1002/(SICI)1521-4095(199906)11:8<605::AID-ADMA605>3.0.CO;2-Q)
26. N. Koch, *ChemPhysChem* **8**(10), 1438 (2007). DOI [10.1002/cphc.200700177](https://doi.org/10.1002/cphc.200700177). URL <http://dx.doi.org/10.1002/cphc.200700177>
27. M.A. Heinrich, J. Pflaum, A.K. Tripathi, W. Frey, M.L. Steigerwald, T. Siegrist, *J. Phys. Chem. C* **111**, 18878 (2007)
28. A. Nelson, *J. Appl. Crystallogr.* **39**(2), 273 (2006). DOI [10.1107/S0021889806005073](https://doi.org/10.1107/S0021889806005073). URL <http://dx.doi.org/10.1107/S0021889806005073>
29. T. Hosokai, M. Horie, T. Aoki, S. Nagamatsu, S. Kera, K.K. Okudaira, N. Ueno, *J. Phys. Chem. C* **112**(12), 4643 (2008). DOI [10.1021/jp710835b](https://doi.org/10.1021/jp710835b). URL <http://dx.doi.org/10.1021/jp710835b>
30. S. Kowarik, A. Gerlach, S. Sellner, F. Schreiber, L. Cavalcanti, O. Kononov, *Phys. Rev. Lett.* **96**(12), 125504 (2006). DOI [10.1103/PhysRevLett.96.125504](https://doi.org/10.1103/PhysRevLett.96.125504). URL <http://link.aps.org/abstract/PRL/v96/e125504>
31. A. Hinderhofer, T. Hosokai, K. Yonezawa, A. Gerlach, K. Kato, K. Broch, C. Frank, J. Novak, S. Kera, N. Ueno, F. Schreiber, *Appl. Phys. Lett.* **101**, 033307 (2012)
32. S. Duhm, G. Heimel, I. Salzmann, H. Glowatzki, R.L. Johnson, A. Vollmer, J.P. Rabe, N. Koch, *Nat. Mater.* **7**(4), 326 (2008). DOI [10.1038/nmat2119](https://doi.org/10.1038/nmat2119). URL <http://dx.doi.org/10.1038/nmat2119>
33. A. Wilke, P. Amsalem, J. Frisch, B. Bröker, A. Vollmer, N. Koch, *Appl. Phys. Lett.* **98**(12), 123304 (2011). DOI [10.1063/1.3571286](https://doi.org/10.1063/1.3571286). URL <http://dx.doi.org/doi/10.1063/1.3571286>
34. Y.L. Huang, W. Chen, H. Huang, D.C. Qi, S. Chen, X.Y. Gao, J. Pflaum, A.T.S. Wee, *J. Phys. Chem. C* **113**(21), 9251 (2009). URL <http://dx.doi.org/10.1021/jp810804t>
35. A.C. Dürr, N. Koch, M. Kelsch, A. Ruehm, J. Ghijsen, R.L. Johnson, J.J. Pireaux, J. Schwartz, F. Schreiber, H. Dosch, A. Kahn, *Phys. Rev. B* **68**, 115428 (2003)
36. J.Q. Zhong, H.Y. Mao, R. Wang, D.C. Qi, L. Cao, Y.Z. Wang, W. Chen, *J. Phys. Chem. C* **115**(48), 23922 (2011). DOI [10.1021/jp208645f](https://doi.org/10.1021/jp208645f). URL <http://pubs.acs.org/doi/abs/10.1021/jp208645f>
37. H. Yamane, Y. Yabuuchi, H. Fukagawa, S. Kera, K.K. Okudaira, N. Ueno, *J. Appl. Phys.* **99**(9), 093705 (2006). DOI [10.1063/1.2192978](https://doi.org/10.1063/1.2192978). URL <http://link.aip.org/link/?JAP/99/093705/1>
38. T. Sueyoshi, H. Kakuta, M. Ono, K. Sakamoto, S. Kera, N. Ueno, *Appl. Phys. Lett.* **96**(9), 093303 (2010). DOI [10.1063/1.3332577](https://doi.org/10.1063/1.3332577). URL <http://link.aip.org/link/?APL/96/093303/1>
39. H.Y. Mao, F. Bussolotti, D.C. Qi, R. Wang, S. Kera, N. Ueno, A.T.S. Wee, W. Chen, *Organic Electronics* **12**(3), 534 (2011). DOI [10.1016/j.orgel.2011.01.003](https://doi.org/10.1016/j.orgel.2011.01.003). URL <http://www.sciencedirect.com/science/article/pii/S1566119911000127>
40. T. Hosokai, H. Machida, A. Gerlach, S. Kera, F. Schreiber, N. Ueno, *Phys. Rev. B* **83**, 195310 (2011). DOI [10.1103/PhysRevB.83.195310](https://doi.org/10.1103/PhysRevB.83.195310). URL <http://link.aps.org/doi/10.1103/PhysRevB.83.195310>

41. F. Schreiber, *Phys. Stat. Sol.* **201**, 1037 (2004)
42. D. Käfer, L. Ruppel, G. Witte, *Phys. Rev. B* **75**(8), 085309 (2007). DOI [10.1103/PhysRevB.75.085309](https://doi.org/10.1103/PhysRevB.75.085309). URL <http://link.aps.org/abstract/PRB/v75/e085309>
43. T.V. Desai, A.R. Woll, F. Schreiber, J.R. Engstrom, *J. Phys. Chem. C* **114**(47), 20120 (2010). DOI [10.1021/jp107518f](https://doi.org/10.1021/jp107518f). URL <http://pubs.acs.org/doi/abs/10.1021/jp107518f>
44. X.N. Zhang, E. Barrera, D.G. de Oteyza, E.D. Souza, H. Dosch, *J. Appl. Phys.* **104**(10), 104308 (2008). DOI [10.1063/1.2977726](https://doi.org/10.1063/1.2977726). URL <http://link.aip.org/link/?JAP/104/104308/1>
45. T.V. Desai, S. Hong, A.R. Woll, K.J. Hughes, A.P. Kaushik, P. Clancy, J.R. Engstrom, *J. Chem. Phys.* **134**(22), 224702 (2011). DOI [10.1063/1.3591965](https://doi.org/10.1063/1.3591965). URL <http://link.aip.org/link/?JCP/134/224702/1>
46. R. Hayakawa, A. Turak, X. Zhang, N. Hiroshiba, H. Dosch, T. Chikyow, Y. Wakayama, *J. Chem. Phys.* **133**(3), 034706 (2010). DOI [10.1063/1.3456733](https://doi.org/10.1063/1.3456733). URL <http://link.aip.org/link/?JCP/133/034706/1>
47. H. Zhu, Q.L. Li, X.J. She, S.D. Wang, *Appl. Phys. Lett.* **98**(24), 243304 (2011). DOI [10.1063/1.3599579](https://doi.org/10.1063/1.3599579). URL <http://link.aip.org/link/?APL/98/243304/1>
48. H. Yang, T.J. Shin, M.M. Ling, K. Cho, C.Y. Ryu, Z. Bao, *J. Am. Chem. Soc.* **127**(33), 11542 (2005). DOI [10.1021/ja052478e](https://doi.org/10.1021/ja052478e). URL <http://pubs.acs.org/doi/abs/10.1021/ja052478e>
49. M.C. Gerstenberg, F. Schreiber, T.Y.B. Leung, G. Bracco, S.R. Forrest, G. Scoles, *Phys. Rev. B* **61**(11), 7678 (2000). DOI [10.1103/PhysRevB.61.7678](https://doi.org/10.1103/PhysRevB.61.7678)
50. S.R. Forrest, *Chem. Rev.* **97**(6), 1793 (1997). DOI [10.1021/cr941014o](https://doi.org/10.1021/cr941014o). URL <http://pubs.acs.org/doi/abs/10.1021/cr941014o>
51. A. Sassella, M. Campione, A. Borghesi, *Rivista del Nuovo Cimento* **31**, 457 (2008)
52. L. Raimondo, M. Moret, M. Campione, A. Borghesi, A. Sassella, *J. Phys. Chem. C* **115**(13), 5880 (2011). DOI [10.1021/jp111754r](https://doi.org/10.1021/jp111754r). URL <http://pubs.acs.org/doi/abs/10.1021/jp111754r>
53. P. Sullivan, T.S. Jones, A.J. Ferguson, S. Heutz, *Appl. Phys. Lett.* **91**(23), 233114 (2007). DOI [10.1063/1.2821229](https://doi.org/10.1063/1.2821229). URL <http://link.aip.org/link/?APL/91/233114/1>
54. P. Peumans, A. Yakimov, S.R. Forrest, *J. Appl. Phys.* **93**(7), 3693 (2003). DOI [10.1063/1.1534621](https://doi.org/10.1063/1.1534621). URL <http://link.aip.org/link/?JAP/93/3693/1>
55. K. Itaka, M. Yamashiro, J. Yamaguchi, M. Haemori, S. Yaginuma, Y. Matsumoto, M. Kondo, H. Koinuma, *Adv. Mater.* **18**(13), 1713 (2006). URL <http://dx.doi.org/10.1002/adma.200502752>
56. M. Kraus, S. Richler, A. Opitz, W. Brütting, S. Haas, T. Hasegawa, A. Hinderhofer, F. Schreiber, *J. Appl. Phys.* **107**(9), 094503 (2010)
57. M. Haemori, J. Yamaguchi, S. Yaginuma, K. Itaka, H. Koinuma, *Jpn. J. Appl. Phys.* **44**(6A), 3740 (2005). DOI [10.1143/JJAP.44.3740](https://doi.org/10.1143/JJAP.44.3740). URL <http://jjap.jsap.jp/link/?JJAP/44/3740/>
58. P. Fenter, F. Schreiber, L. Zhou, P. Eisenberger, S.R. Forrest, *Phys. Rev. B* **56**, 3046 (1997). URL <http://dx.doi.org/10.1103/PhysRevB.56.3046>
59. D.E. Hooks, T. Fritz, M.D. Ward, *Adv. Mater.* **13**, 227 (2001). DOI [10.1002/1521-4095\(200102\)13:4<227::AID-ADMA227>3.0.CO;2-P](https://doi.org/10.1002/1521-4095(200102)13:4<227::AID-ADMA227>3.0.CO;2-P). URL [http://dx.doi.org/10.1002/1521-4095\(200102\)13:4<227::AID-ADMA227>3.0.CO;2-P](http://dx.doi.org/10.1002/1521-4095(200102)13:4<227::AID-ADMA227>3.0.CO;2-P)
60. L. Kilian, A. Hauschild, R. Temirov, S. Soubatch, A. Schöll, A. Bendounan, F. Reinert, T.L. Lee, F.S. Tautz, M. Sokolowski, E. Umbach, *Phys. Rev. Lett.* **100**, 136103 (2008). DOI [10.1103/PhysRevLett.100.136103](https://doi.org/10.1103/PhysRevLett.100.136103). URL <http://link.aps.org/doi/10.1103/PhysRevLett.100.136103>
61. T.B. Singh, N.S. Sariciftci, H. Yang, L. Yang, B. Plochberger, H. Sitter, *Appl. Phys. Lett.* **90**(21), 213512 (2007). DOI [10.1063/1.2743386](https://doi.org/10.1063/1.2743386). URL <http://link.aip.org/link/?APL/90/213512/1>
62. S. Yim, T.S. Jones, *Appl. Phys. Lett.* **94**(2), 021911 (2009). DOI [10.1063/1.3072805](https://doi.org/10.1063/1.3072805). URL <http://link.aip.org/link/?APL/94/021911/1>
63. I. Salzmann, S. Duhm, R. Opitz, R.L. Johnson, J.P. Rabe, N. Koch, *J. Appl. Phys.* **104**(11), 114518 (2008). DOI [10.1063/1.3040003](https://doi.org/10.1063/1.3040003). URL <http://link.aip.org/link/?JAP/104/114518/1>
64. W. Chen, H. Zhang, H. Huang, L. Chen, A.T.S. Wee, *ACS Nano* **2**(4), 693 (2008). DOI [10.1021/nn800033z](https://doi.org/10.1021/nn800033z). URL <http://pubs.acs.org/doi/abs/10.1021/nn800033z>

65. J.Q. Zhong, H. Huang, H.Y. Mao, R. Wang, S. Zhong, W. Chen, *J. Chem. Phys.* **134**(15), 154706 (2011). DOI [10.1063/1.3582789](https://doi.org/10.1063/1.3582789). URL <http://link.aip.org/link/?JCP/134/154706/1>
66. U. Heinemeyer, R. Scholz, L. Gisslén, M.I. Alonso, J.O. Ossó, M. Garriga, A. Hinderhofer, M. Kytka, S. Kowarik, A. Gerlach, F. Schreiber, *Phys. Rev. B* **78**, 085210 (2008). URL <http://dx.doi.org/10.1103/PhysRevB.78.085210>
67. A.C. Dürr, F. Schreiber, K.A. Ritley, V. Kruppa, J. Krug, H. Dosch, B. Struth, *Phys. Rev. Lett.* **90**, 016104 (2003)
68. R. Scholz, L. Gisslén, B.E. Schuster, M.B. Casu, T. Chassé, U. Heinemeyer, F. Schreiber, *J. Chem. Phys.* **134**, 014504 (2011). URL <http://dx.doi.org/doi:10.1063/1.3514709>
69. J. Wagner, M. Gruber, A. Wilke, Y. Tanaka, K. Topczak, A. Steindamm, U. Hörmann, A. Opitz, Y. Nakayama, H. Ishii, J. Pflaum, N. Koch, W. Brütting, *J. Appl. Phys.* **111**(5), 054509 (2012). DOI [10.1063/1.3692050](https://doi.org/10.1063/1.3692050). URL <http://link.aip.org/link/?JAP/111/054509/1>
70. R.R. Lunt, N.C. Giebink, A.A. Belak, J.B. Benziger, S.R. Forrest, *J. Appl. Phys.* **105**(5), 053711 (2009). DOI [10.1063/1.3079797](https://doi.org/10.1063/1.3079797). URL <http://link.aip.org/link/?JAP/105/053711/1>
71. A. Hinderhofer, A. Gerlach, K. Broch, T. Hosokai, K. Yonezawa, K. Kato, S. Kera, N. Ueno, F. Schreiber, *J. Phys. Chem. C* **117**(2), 1053 (2013). DOI [10.1021/jp3106056](https://doi.org/10.1021/jp3106056). URL <http://pubs.acs.org/doi/abs/10.1021/jp3106056>
72. J.L. de Boer, S. van Smaalen, V. Petricek, M. Dusek, M.A. Verheijen, G. Meijer, *Chem. Phys. Lett.* **219**(5–6), 469 (1994). DOI [DOI:10.1016/0009-2614\(94\)00110-3](https://doi.org/10.1016/0009-2614(94)00110-3). URL <http://www.sciencedirect.com/science/article/B6TFN-44J6FC9-M4/2/165963913b89bd08a6214011d478c2c0>
73. R.W. Lof, M.A. van Veenendaal, B. Koopmans, H.T. Jonkman, G.A. Sawatzky, *Phys. Rev. Lett.* **68**, 3924 (1992). DOI [10.1103/PhysRevLett.68.3924](https://doi.org/10.1103/PhysRevLett.68.3924). URL <http://link.aps.org/doi/10.1103/PhysRevLett.68.3924>
74. S. Krause, Determination of the transport levels in thin films of organic semiconductors. Ph.D. thesis, Universität Würzburg (2008)
75. J.H. Weaver, J.L. Martins, T. Komeda, Y. Chen, T.R. Ohno, G.H. Kroll, N. Troullier, R.E. Haufler, R.E. Smalley, *Phys. Rev. Lett.* **66**, 1741 (1991). DOI [10.1103/PhysRevLett.66.1741](https://doi.org/10.1103/PhysRevLett.66.1741). URL <http://link.aps.org/doi/10.1103/PhysRevLett.66.1741>
76. S. Hasegawa, T. Miyamae, K. Yakushi, H. Inokuchi, K. Seki, N. Ueno, *Phys. Rev. B* **58**, 4927 (1998). DOI [10.1103/PhysRevB.58.4927](https://doi.org/10.1103/PhysRevB.58.4927). URL <http://link.aps.org/doi/10.1103/PhysRevB.58.4927>
77. O.V. Molodtsova, M. Knupfer, *J. Appl. Phys.* **99**(5), 053704 (2006). DOI [10.1063/1.2175468](https://doi.org/10.1063/1.2175468). URL <http://link.aip.org/link/?JAP/99/053704/1>
78. T. Liebsch, O. Plotzke, F. Heiser, U. Hergenhausen, O. Hemmers, R. Wehlitz, J. Viehhaus, B. Langer, S.B. Whitfield, U. Becker, *Phys. Rev. A* **52**, 457 (1995). DOI [10.1103/PhysRevA.52.457](https://doi.org/10.1103/PhysRevA.52.457). URL <http://link.aps.org/doi/10.1103/PhysRevA.52.457>
79. H. Fukagawa, H. Yamane, T. Kataoka, S. Kera, M. Nakamura, K. Kudo, N. Ueno, *Phys. Rev. B* **73**, 245310 (2006). DOI [10.1103/PhysRevB.73.245310](https://doi.org/10.1103/PhysRevB.73.245310). URL <http://link.aps.org/doi/10.1103/PhysRevB.73.245310>
80. S. Kera, H. Yamane, N. Ueno, *Prog. Surf. Sci.* **84**, 135 (2009). DOI [10.1016/j.progsurf.2009.03.002](https://doi.org/10.1016/j.progsurf.2009.03.002). URL <http://www.sciencedirect.com/science/article/pii/S007968160900029X>
81. P. He, S. Bao, C. Yu, Y. Xu, *Surf. Sci.* **328**(3), 287 (1995). DOI [10.1016/0039-6028\(95\)00036-4](https://doi.org/10.1016/0039-6028(95)00036-4). URL <http://www.sciencedirect.com/science/article/pii/0039602895000364>
82. R. Tycko, G. Dabbagh, R.M. Fleming, R.C. Haddon, A.V. Makhija, S.M. Zahurak, *Phys. Rev. Lett.* **67**, 1886 (1991). DOI [10.1103/PhysRevLett.67.1886](https://doi.org/10.1103/PhysRevLett.67.1886). URL <http://link.aps.org/doi/10.1103/PhysRevLett.67.1886>
83. H. Fukagawa, S. Kera, T. Kataoka, S. Hosoumi, Y. Watanabe, K. Kudo, N. Ueno, *Adv. Mater.* **19**(5), 665 (2007). URL <http://dx.doi.org/10.1002/adma.200601678>
84. M.T. Greiner, M.G. Helander, W.M. Tang, Z.B. Wang, J. Qiu, Z.H. Lu, *Nat. Mater.* **11**(1), 76 (2012). DOI [10.1038/nmat3159](https://doi.org/10.1038/nmat3159). URL <http://dx.doi.org/10.1038/nmat3159>
85. S. Braun, W.R. Salaneck, M. Fahlman, *Adv. Mater.* **21**(14–15), 1450 (2009). DOI [10.1002/adma.200802893](https://doi.org/10.1002/adma.200802893). URL <http://dx.doi.org/10.1002/adma.200802893>

86. H. Vazquez, W. Gao, F. Flores, A. Kahn, *Phys. Rev. B* **71**(4), 041306 (2005). DOI [10.1103/PhysRevB.71.041306](https://doi.org/10.1103/PhysRevB.71.041306). URL <http://link.aps.org/abstract/PRB/v71/e041306>
87. M. Linares, D. Beljonne, J. Cornil, K. Lancaster, J.L. Brédas, S. Verlaak, A. Mityashin, P. Heremans, A. Fuchs, C. Lennartz, J. Idé, R. Méreau, P. Aurel, L. Ducasse, F. Castet, *J. Phys. Chem. C* **114**(7), 3215 (2010). DOI [10.1021/jp910005g](https://doi.org/10.1021/jp910005g). URL <http://pubs.acs.org/doi/abs/10.1021/jp910005g>
88. J. Ivanco, *Thin Solid Films* **520**(11), 3975 (2012). DOI [10.1016/j.tsf.2012.01.035](https://doi.org/10.1016/j.tsf.2012.01.035). URL <http://www.sciencedirect.com/science/article/pii/S0040609012000739>